Submitted to the 29th International Conference on High-Energy Physics ICHEP98,
Vancouver, Canada, July 1998
(Revised on 7/7/98)

A Search for Leptoquark Bosons in DIS at High Q^2 at HERA

H1 Collaboration

Abstract

A search for new bosons possessing couplings to lepton-quark pairs is performed in the H1 experiment at HERA using 1994→1997 data corresponding to an integrated luminosity of 37 pb $^{-1}$. The very high Q^2 neutral (NC) and charged (CC) current data are first compared to Standard Model expectations from deep inelastic scattering. The deviations in the Q^2 spectrum previously observed in the 1994→1996 data at $Q^2 \gtrsim 15000$ GeV^2 remain, though with less significance. No significant clustering in the mass spectra is observed with the 1997 data alone. The data are used to constrain the direct s-channel production of first generation leptoquarks. Compared with earlier HERA results, the exclusion limits are considerably improved for leptoquarks which could be produced via e^+-*valence quark* fusion and extend beyond the coupling-mass domain covered so far at other colliders for a small branching ratio to e^+q. For a branching ratio as small as 10%, masses up to 255 GeV are ruled out by the present analysis for a Yukawa coupling of electromagnetic size for the leptoquark to e^+u pair. The analysis is then extended to cover also leptoquarks with mixed couplings allowing for decays into leptons of the second or third generation. None of the $\mu + jet$ or $\tau + jet$ event candidates are found to be compatible with the two body decay hypothesis of a leptoquark. Constraints are set on the Yukawa coupling involving the τ lepton for a mass range extending beyond the domain presently covered at other colliders.

Abstract: 579
Parallel sessions: 10
Plenary sessions: 12

1 Introduction

The ep collider HERA offers the unique possibility to search for s-channel production of new scalar particles which couple to lepton-parton pairs. Examples are leptoquark (LQ) colour triplet bosons which appear naturally in various unifying theories beyond the Standard Model (SM) such as Grand Unified Theories and Superstring inspired E_6 models, and in some Compositeness and Technicolour models. They could be singly produced by the fusion of the 27.5 GeV initial state lepton with a quark of the 820 GeV incoming proton, with masses up to the kinematic limit of $\sqrt{s_{ep}} \simeq 300$ GeV.

The interest in such new scalar bosons has been considerably renewed recently following the observation by the H1 [1] and ZEUS [2] experiments of an excess of events at very high masses and Q^2, above expectations from Standard Model (SM) neutral current (NC) and charged current (CC) deep-inelastic scattering (DIS). These early results were based on data samples collected from 1994 to 1996. Of particular interest was the apparent "clustering" of outstanding events at masses around 200 GeV observed in H1 which, although not specifically supported by ZEUS observations [3, 4], has motivated considerable work on leptoquark constraints and phenomenology [5] extending beyond the original effective model of Buchmüller-Rückl-Wyler (BRW) [6].

In this paper, we first present a comparison of the H1 measurements at very high masses and Q^2 with SM expectations using all available e^+p data collected from 1994 to 1997. The mass and angular distributions from NC- and CC-like events are then used in the context of a leptoquark search to set constraints on first generation leptoquarks. The search for leptoquarks is further extended to allow for mixing in the lepton sector leading to decays involving second or third generation leptons. The total integrated luminosity $\mathcal{L}$ amounts to 37 pb $^{-1}$, an increase in statistics of a factor $\sim\ 2.6$ compared to previous analysis at very high Q^2 [1] and a factor ~ 13 compared to previous leptoquark searches at HERA [7, 8].

2 Phenomenology

The search for first generation leptoquarks at HERA involves the analysis of DIS-like events at very high Q^2. In the s-channel, a leptoquark is produced at fixed mass $M = \sqrt{s_{ep}x}$ where x is the momentum fraction of the proton carried by the incoming quark. The production cross section σ_{LQ} depends on the quark momentum density in the proton and approximately scales with λ^2 where λ is the Yukawa coupling to the lepton-quark pair. The scalar resonance which can then decay into $e + q$ or $\nu + q$ is expected to have a very narrow intrinsic width $\Gamma = \lambda^2 M/16\pi$ and the decays into a lepton and a quark jet lead to signatures which are practically indistinguishable event-by-event from SM neutral and charged current deep inelastic scattering.

Statistically, the new signal may however be identified as a resonance peak in the invariant mass distribution, with events in the peak possessing a specific angular distribution of the decay products. Scalar leptoquarks decay isotropically in their centre of mass (CM) frame leading to a flat $\mathrm{d}\sigma\,/\,\mathrm{d}y$ spectrum where $y = \frac{1}{2}(1+\cos\theta^*)$ is the Bjorken scattering variable in DIS and θ^* is the decay polar angle in the leptoquark CM frame. This is markedly different from the $\mathrm{d}\sigma\,/\,\mathrm{d}y \sim y^{-2}$ distribution expected at fixed x for the dominant t-channel photon exchange in neutral current DIS events [1]. Hence, the signal of first generation leptoquarks will be most prominent at high y.

In contrast, the $e + q \rightarrow LQ \rightarrow \mu + q'$ or $\tau + q'$ processes lead to exotic signatures which are expected to be essentially background free at high transverse momentum of the final state lepton.

In this paper the leptoquark search will be discussed either in the strict context of the BRW phenomenological ansatz [6] where the decay branching ratios are fixed by the model, or in the context of generic models allowing for arbitrary branching ratios. The BRW model considers all possible scalar (S_I) and vector (V_I) leptoquarks of weak isospin *I* with dimensionless couplings $\lambda_{ij}^{L,R}$ to lepton-quark pairs, where *i* and *j* indices denote lepton and quark generations respectively and *L* or *R* is the chirality of the lepton. The general effective Lagrangian which is introduced obeys the symmetries of the SM. There are 10 different leptoquark isospin multiplets, with couplings to left or right handed fermions, among which there are 5 scalar leptoquark isospin families. These are listed in Table 1. The search must be restricted to pure chiral cou-

$F = -2$	Prod./decay	$\mathcal{B}(e^+q)$	$F = 0$	Prod./decay	$\mathcal{B}(e^+q)$
${}^{-1/3}S_0^*$	$e_R^+\bar{u}_R \rightarrow e^+\bar{u}$	$1/2$	${}^{-5/3}S_{1/2}^*$	$e_R^+u_R \rightarrow e^+u$	1
	$e_L^+\bar{u}_L \rightarrow e^+\bar{u}$	1		$e_L^+u_L \rightarrow e^+u$	1
${}^{-4/3}\tilde{S}_0^*$	$e_L^+\bar{d}_L \rightarrow e^+\bar{d}$	1	${}^{-2/3}S_{1/2}^*$	$e_L^+d_L \rightarrow e^+d$	1
${}^{-4/3}S_1^*$	$e_R^+\bar{d}_R \rightarrow e^+\bar{d}$	1	${}^{-2/3}\tilde{S}_{1/2}^*$	$e_R^+d_R \rightarrow e^+d$	1
${}^{-1/3}S_1^*$	$e_R^+\bar{u}_R \rightarrow e^+\bar{u}$	$1/2$			

Table 1: Scalar leptoquarks isospin families in the Buchmüller-Rückl-Wyler model. These LQ will be in the following indexed with the chirality of the incoming *electron* which could allow their production, e.g. the $\tilde{S}_0^*$ will be denoted by $\tilde{S}_{0,R}^*$.

plings of the leptoquarks given that deviations from lepton universality in helicity suppressed pseudoscalar meson decays have not been observed [9, 10]. This restriction to couplings with either left- (λ^L) or right-handed (λ^R) leptons (i.e. $\lambda^L \cdot \lambda^R \sim 0$), affects only two scalar leptoquarks (S_0 and $S_{1/2}$). We make use of the so-called Aachen nomenclature and classification scheme [11]. We make the simplifying assumptions that one of the leptoquark multiplets is produced dominantly and that the mass eigenstates within the leptoquark isospin doublets and triplets are degenerate in mass.

3 The H1 detector

A detailed description of the H1 detector can be found elsewhere [12]. Here we describe only the components relevant for the present analysis in which the final state of the events involves either a positron[2] with high transverse energy or a large amount of hadronic transverse energy flow.

[1] At high momentum transfer, Z^0 exchange is no longer negligible and contributes to less pronounced differences in the y spectra between leptoquark signal and DIS background.

[2] The analysis does not distinguish explicitly between e^+ and e^-.

The positron energy and angle are measured in a liquid argon (LAr) sampling calorimeter [13] covering the polar angular[3] range $4^\circ \leq \theta \leq 154^\circ$ and all azimuthal angles. The granularity is optimized to provide fine and approximately uniform segmentation in laboratory pseudorapidity and azimuthal angle ϕ. It consists of a lead/argon electromagnetic section followed by a stainless steel/argon hadronic section. Electromagnetic shower energies are measured with a resolution of $\sigma(E)/E \simeq 12\%/\sqrt{E/\text{ GeV}} \oplus 1\%$ and pion induced hadronic energies with $\sigma(E)/E \simeq 50\%/\sqrt{E/\text{ GeV}} \oplus 2\%$ after software energy weighting. These resolutions were measured in test beams with electron energies up to 166 GeV [14, 15] and pion energies up to 205 GeV [15]. The absolute energy scales are known to 3% and 4% for electromagnetic and hadronic energies respectively. The angular resolution on the positron measured from the electromagnetic shower in the calorimeter varies from ~ 2 mrad below 30° to $\lesssim 5$ mrad at larger angles. A lead/scintillating-fibre backward calorimeter [16] extends the coverage[4] at larger angles ($153^\circ \leq \theta \lesssim 178^\circ$).

Located inside the calorimeters is the tracking system which is used here to determine the interaction vertex. The main components of this system are central drift and proportional chambers ($25^\circ \leq \theta \leq 155^\circ$), a forward track detector ($7^\circ \leq \theta \leq 25^\circ$) and a backward drift chamber[3]. The tracking chambers and calorimeters are surrounded by a superconducting solenoid providing a uniform field of 1.15 T parallel to the z axis within the detector volume. The instrumented iron return yoke surrounding this solenoid is used to measure leakage of hadronic showers and to recognize muons. The luminosity is determined from the rate of the Bethe-Heitler $ep \to ep\gamma$ bremsstrahlung measured in a luminosity monitor. This consists of a positron tagger (e-tagger) and a photon tagger (γ-tagger), located -33 m and -103 m respectively from the interaction point.

The increase of statistics accumulated in 1997 allowed for the first time an *in situ* calibration of the electromagnetic section of the LAr calorimeter to be performed exploiting [18] the kinematic constraints of NC DIS and elastic QED Compton events. The large amount of data with a lepton scattered in the central wheels of the LAr allowed a very fine calibration in this region leading to a precision of 1% for θ between 80° and 150° on the electromagnetic energy scale. Moreover, in the forward region of the LAr calorimeter, the calibration scale has been globally improved and it could be checked that the absolute calibration of positron energies ranges within the $\pm 3\%$ systematics originally estimated from extrapolations based on CERN test beam results. All analysis described in the following rely on this updated calibration.

4 SM Background and Leptoquark Signal Simulation

The calculation of the Standard Model expectation for NC and CC DIS ep scattering is performed using the parton model in the approximation of single γ/Z and W boson exchange, with NC and CC cross sections containing a description of the proton in terms of scale dependent structure functions. The structure functions are expressed in terms of parton densities and, following [1], these are taken here from the Martin-Roberts-Stirling MRS (H) [19] parametrizations. The parton densities are evolved to the high Q^2 relevant for this analysis using the next-to-leading order DGLAP equations [20]. The Monte Carlo event generator DJANGO [21] which

[3] The z axis is taken to be in the direction of the incident proton, the forward direction, and the origin of coordinates is the nominal ep interaction point.

[4] The detectors in the backward region were upgraded in 1995 by the replacement of the lead/scintillator tile calorimeter [17] and a proportional chamber.

follows such an approach is used for the comparison with data. This generator includes the QED first order radiative corrections, and emission of real bremsstrahlung photons [22] and a modelling of the emission of QCD radiation via ARIADNE [23]. The ARIADNE generator makes use of the Colour Dipole Model [24] to simulate QCD radiation to all orders and string fragmentation [25] to generate the hadronic final state.

The contributions from all background processes [1] which could give rise to events with true or misidentified isolated leptons at high E_T or to events with a large $P_{T,miss}$ were evaluated. In particular, direct and resolved photoproduction processes were modelled using the PYTHIA generator [26]. It is based on leading order QCD matrix elements and includes initial and final state parton showers calculated in the leading logarithm approximation, and string fragmentation [25]. The renormalization and factorization scales are both set to P_T^2, P_T being the transverse momentum of the jets emerging out of the hard subprocess. The GRV (G) leading order parton densities in the proton (photon) are used [27].

For Monte Carlo simulation of leptoquark signals, we make use of the LEGO event generator [28] which was described in more detail in [7]. It takes into account initial state QED radiation and QCD corrections in the initial and final states, and it corrects properly the kinematics at the decay vertex for effects of the parton shower masses.

A complete Monte Carlo simulation of the H1 detector response is performed for all signal and background processes. In addition, the following experimental errors are propagated as systematic errors on the mean SM expectations :

- the uncertainty on the integrated luminosity ($\pm 2.3\%$);
- the uncertainty on the absolute calibration of the calorimeters for electromagnetic energies, ranging between $\pm 1\%$ in the central wheels and $\pm 3\%$ in the forward region of the LAr calorimeter;
- the uncertainty on the absolute calibration of the calorimeters for hadronic showers ($\pm 4\%$).

In addition, a 7% "theoretical" uncertainty on the predicted NC DIS cross section originates (see detailed discussion in [1]) mainly from contributions of parton density distributions extracted from "QCD fits", of the value of the strong coupling constant α_s and, to a lesser extent, from the higher order QED corrections. For CC DIS processes which are mainly induced by d quarks, this uncertainty varies with Q^2 and ranges between 7% and $\simeq 20\%$ at the highest Q^2 considered here. All analyses described in the following sections have been repeated with an independent shift of the central values by ± 1 standard deviation of each of the experimental and theoretical sources of errors. The overall systematic error of the standard DIS model prediction is determined as the quadratic sum of the resulting errors and of the statistical error on the Monte Carlo simulation.

5 Event Selection and Kinematics

5.1 DIS-like signatures

The search for first generation leptoquarks relies on an essentially inclusive event selection. This will allow us to extend, with higher statistics, the general comparison with standard DIS model expectations of the M, y and Q^2 spectra as performed in [1].

The analysis considers datasets taken under running conditions and accepted by LAr trigger requirements identical to that of [1]. The rejection of background from cosmic rays and from "halo" muons associated with the proton beam mainly relies on constraints on the event timing relative to the nominal time of the beam bunch crossings. Beam-wall and beam-residual gas interactions are furthermore suppressed by requiring a primary vertex in the range $\mid z - \bar{z} \mid < 40$ cm where $\bar{z}$ varies within ± 5 cm around $z = 0$ depending on the HERA beam settings.

The **selection of NC DIS-like events** at high Q^2 essentially relies on calorimetric information for electron finding and energy-momentum conservation requirements:

1. an isolated positron with $E_{T,e} > 15$ GeV ($E_{T,e} = E_e \sin\theta_e$), found within the polar angular range $5° \leq \theta_e \leq 145°$; the positron energy cluster should contain more than 98% of the LAr energy found within a pseudorapidity-azimuthal cone of opening $\sqrt{(\Delta\eta_e)^2 + (\Delta\phi_e)^2} = 0.25$ where $\eta_e = -\ln\tan\frac{\theta_e}{2}$; at least one charged track is required within the positron isolation cone;

2. a total transverse momentum balance $P_{T,miss}/\sqrt{E_{T,e}} \leq 4\sqrt{\text{GeV}}$ where $P_{T,miss}$ is obtained as the sum $P_{T,miss} \equiv \sqrt{\left(\sum E_{x,i}\right)^2 + \left(\sum E_{y,i}\right)^2}$ over all energy deposits i in the calorimeters, with $E_{x,i} = E_i \sin\theta_i \cos\phi_i$ and $E_{y,i} = E_i \sin\theta_i \sin\phi_i$;

3. a limited momentum loss in the direction of the incident positron, $40 \leq \sum(E - P_z) \leq 70$ GeV, where $\sum(E - P_z) \equiv \sum(E_i - E_{z,i})$ with $E_{z,i} = E_i \cos\theta_i$.

The identification of positron induced showers relies on detailed knowledge of the expected lateral and longitudinal shower properties [14, 18]. The efficiency for the detection of positrons exceeds 90% everywhere within the acceptance cuts, the main losses being due to showers developing through the inactive material between calorimeter modules. The cut (2) makes possible a very efficient NC DIS selection up to the highest Q^2 by taking into account the natural scale of the hadronic energy resolution. The cut (3) retains more than 90% of NC DIS events and exploits the fact that by energy-momentum conservation, the $\sum(E - P_z)$ distribution for NC DIS events is peaked at $2E_e^0$. It rejects events where a very hard collinear γ is emitted by the initial state positron.

To calculate the appropriate DIS Lorentz invariants Q^2, y and $M = \sqrt{xs}$, two different sets of estimators are used to cope with projective ϕ cracks separating octants of the LAr calorimeter. Firstly, use is made of only the measurement of the scattered positron when the impact at the inner surface of the calorimeter of the charged track associated to the positron is at more than $\mid \phi_e - \phi_{crack} \mid = 2°$ from the nearest crack:

$$M_e = \sqrt{s x_e} = \sqrt{\frac{Q_e^2}{y_e}}, \quad Q_e^2 = \frac{E_{T,e}^2}{1 - y_e}, \quad y_e = 1 - \frac{E_e - E_e\cos\theta_e}{2E_e^0} \quad .$$

This method will henceforth be denoted the e-method. Secondly use is made of only the reconstructed angles θ_e and θ_h of the positron and hadronic final state when the positron cluster energy measurement deteriorates in the range $1° < \mid \phi_e - \phi_{crack} \mid < 2°$. Using $\alpha_e = \tan(\theta_e/2) = (E_e - E_{z,e})/E_{T,e}$, and $\alpha_h = \tan(\theta_h/2) = \sum(E_i - E_{z,i})/\sqrt{(\sum E_{x,i})^2 + (\sum E_{y,i})^2}$, where the summations are over all energy deposits of the hadronic final state, then [29] :

$$M_{2\alpha} = \sqrt{\frac{s}{\alpha_e\alpha_h}\frac{E_e^0}{E_p}}, \quad Q_{2\alpha}^2 = \frac{E_e^0}{E_p}\frac{s}{\alpha_e(\alpha_e + \alpha_h)}, \quad y_{2\alpha} = \frac{\alpha_h}{\alpha_e + \alpha_h}.$$

This method will henceforth be denoted the 2α-method. A fiducial cut is applied to reject event candidates with $\mid \phi_e - \phi_{crack} \mid < 1°$.

In the parton model, the variable x is interpreted as the momentum fraction carried by the parton coming from the proton entering the hard subprocess. The centre of mass energy of the positron-parton collision is M. The variable y is related to the polar scattering angle θ_e^* of the positron relative to the incident proton in the centre of mass frame of the positron-parton collision according to $y = (1 + \cos\theta_e^*)/2$.

In addition to the cuts (1) to (3) above, the analysis is restricted to the kinematic range $Q^2 > 2500$ GeV^2 and $0.1 < y < 0.9$. The resolution in M_e degrades with decreasing y_e ($\delta M_e/M_e \propto 1/y_e$) and so the low y domain is excluded. Excluding the high y values suppresses the photoproduction background and also avoids the region where QED radiative effects are largest for the e-method. For this kinematic range, the NC trigger efficiency exceeds 96% and is consistent with 100% to within experimental error. Following [1], a minimal set of cuts [18] designed to specifically eliminate photoproduction, $\gamma\gamma$ and QED Compton processes is applied which induces only small ($< 5\%$) efficiency loss for NC DIS-like processes.

Applying all above NC selection criteria, 1297 DIS event candidates are accepted using the e-method for the calculation of the kinematic cuts. This is in good agreement with the expectation of 1276 ± 98 events expected from standard NC DIS. The background contamination from non-NC DIS processes is estimated to be below 0.1% [1] and is henceforth neglected. Fig. 1 shows the two dimensional distribution of y_e against M_e for the NC candidates, together with four isolines in Q^2.

The inclusive **selection of CC DIS-like events** requires:

1. no $e^{\pm}$ candidate with $E_T > 5$ GeV found in the LAr calorimeter, with the same electron identification algorithm as used to select NC DIS candidates;

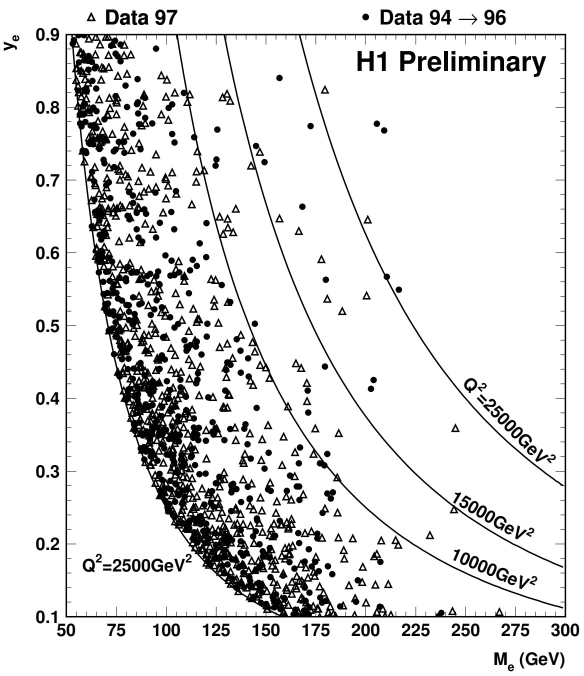

Figure 1: Selected NC DIS candidate events in the y_e - M_e plane; open triangles (resp. closed dots) correspond to 1997 (resp. 1994 to 1996) data events; four contours of fixed Q^2 are shown.

2. the total missing transverse momentum $P_{T,miss} = P_{T,h} > 50$ GeV.

These cuts eliminate the photoproduction and NC DIS background and are similar to those of [1]. To deal with specific background sources to CC DIS, it is required that there should be no isolated high P_T track found within the angular range $10° \leq \theta \leq 145°$ and with $P_T > 10$ GeV. This suppresses in particular eventual background from single W boson production and causes negligible efficiency losses for the CC DIS selection. The remaining contamination from single W production is below 0.02% (95% confidence level) within the analysis cuts.

The DIS Lorentz invariants Q^2, y and M are calculated using the Jacquet-Blondel ansatz [30] by summing over all measured final state hadronic energy deposits using:

$$M_h = \sqrt{\frac{Q_h^2}{y_h}}, \quad Q_h^2 = \frac{P_{T,h}^2}{1 - y_h}, \quad y_h = \frac{\sum (E - P_z)}{2E_e^0}.$$

This method will henceforth be denoted the h-method.

In addition to the cuts (1) and (2) above, the analysis is restricted to the kinematic range $y_h < 0.9$. The resolutions in both M_h and Q_h^2 degrade with increasing y (both $\delta M_h/M_h$ and $\delta Q_h^2/Q_h^2$ behave as $\propto 1/(1 - y_h)$ for $y_h \sim 1$) and so the high y_h domain is excluded. Together with the requirement of cut (2) this restricts implicitly the kinematic range to $Q_h^2 > 2500$ GeV^2. Throughout this range, the CC trigger efficiency is $\gtrsim 90\%$. Following this CC selection, 100 DIS event candidates are accepted in good agreement with the standard CC DIS expectation of 95.3 ± 16.7 events.

For the specific leptoquark search, we will also consider a less stringent $P_{T,miss}$ requirement of $P_{T,miss} > 30$ GeV for which we observe 210 events at $M_h > 50$ GeV, in good agreement with the CC DIS expectation of 193.7 ± 28.5 events.

5.2 High P_T Lepton Signatures

For **leptoquarks coupling to a second generation lepton**, leading to $\mu + q$ final states, we start from a CC-like selection with $P_{T,miss} > 25$ GeV (where $P_{T,miss}$ is calculated from calorimetric quantities) and simply require as a muon signature an isolated charged track with transverse momentum $P_T > 10$ GeV linked to the primary vertex. Only four "outstanding" $\mu + jet$ events are observed after applying these basic requirements. All four are amongst the high P_T lepton events discussed in [31]. Considering further the kinematic constraints of a $2 \rightarrow 2$ body process, the selection of $LQ \rightarrow \mu q$ candidates requires the high P_T isolated track to be within $(\Delta\theta < 30°, \Delta\Phi < 15°)$ around the "muon" angle deduced using the hadronic energy flow. As seen in Fig. 2, these criteria induce a minute efficiency loss for a leptoquark signal simulation. The actual loss was estimated to be $\simeq 4\%$ using real NC-like data by searching for the charged track angles associated with the positron candidate as deduced using the hadronic energy flow.

We observe no candidate satisfying the $LQ \rightarrow \mu + jet$ selection. In particular, the $e^+p \rightarrow \mu^+X$ outstanding events discussed in [31] fail significantly the kinematic constraints for $eq \rightarrow LQ \rightarrow \mu q'$ processes as can be seen in Fig. 2.

For **leptoquarks coupling to a third generation lepton** leading to $\tau + q$ final states, the analysis is restricted to hadronic decays of the τ (the $\tau^+ \rightarrow \mu^+\nu_\mu\bar{\nu_\tau}$ are included in the above $\mu + q$ analysis since the τ decay products are strongly boosted in the τ direction; the $\tau^+ \rightarrow$

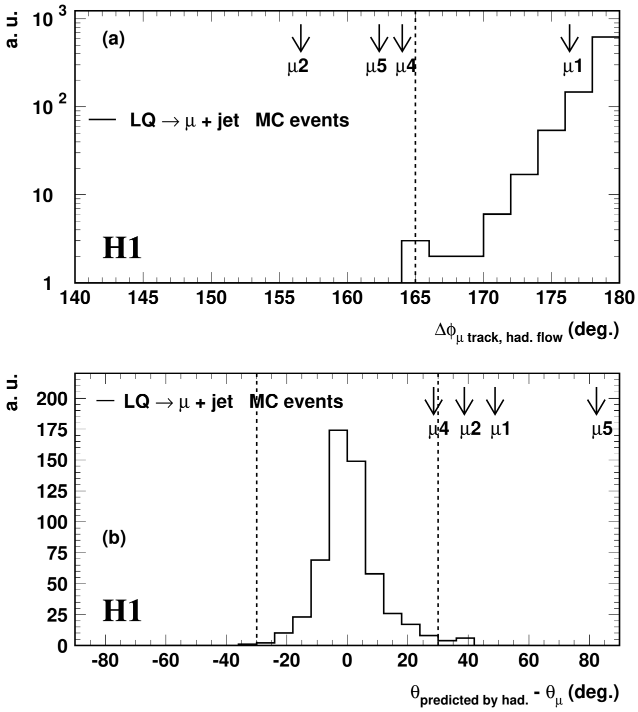

Figure 2: (a) Azimuthal opening between the track associated to the high P_T muon in $e + p \to \mu + jet$ events and the hadronic energy flow; (b) Polar angle opening between the muon track and the final state lepton angle predicted from the hadronic energy flow for a $2 \to 2$ body process. Arrows indicate the $\Delta\phi$ and $\Delta\theta$ values for the "outstanding" events reported in [31]. Histograms represent the expected distributions of these variables for $LQ \to \mu + q$ Monte-Carlo events.

$e^+\nu_e\bar{\nu_\tau}$ channel is not considered here). The identification of "pencil-like" jets induced by hadronic decays of τ requires that the jet invariant mass satisfies $M_{jet} \leq 7$ GeV and has a low multiplicity, namely $1 \leq N_{tracks} \leq 3$, N_{tracks} being the number of vertex fitted tracks with $P_T > 0.15$ GeV in the jet identification cone. Inclusive τ + jet signatures, where the τ lepton decays into hadrons, are selected by requiring that :

1. no $e^\pm$ candidate with $E_T > 5$ GeV is found in the LAr calorimeter, using the same electron identification algorithm as used for the selection of NC DIS-like events described in 5.1;

2. two jets are found in the angular range $7° < \theta < 145°$ using a cone algorithm in the laboratory frame with a radius $\sqrt{(\Delta\eta)^2 + (\Delta\Phi)^2} = 1$, with a transverse momentum $P_T > 30$ GeV; one of these jets must satisfy the "loose" τ-jet identification criteria described above;

3. there is at most a small amount of energy deposited in the backward calorimeters, $E_{back} < 7.5$ GeV;

4. the impact point of the leading track associated to the τ jet at the inner surface of the LAr calorimeter must be at least $2°$ apart in azimuth from each of the eight ϕ cracks of the LAr;

5. the leading track associated to the τ jet carries a large enough fraction $E_{track}/E_{\tau-jet} > 10\%$ of the jet energy $E_{\tau-jet}$;

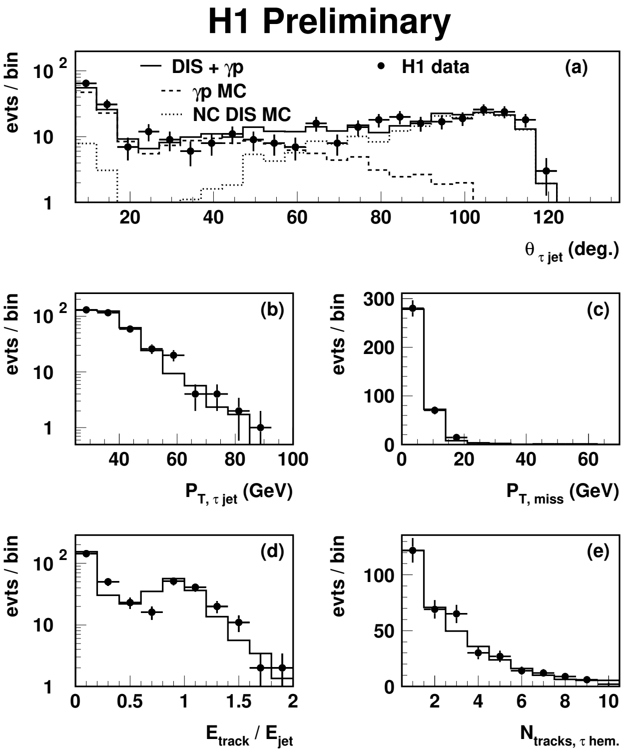

Figure 3: Distributions of (a) the polar angle $\theta_{\tau-jet}$ of the τ jet candidate; (b) the transverse momentum of the τ jet; (c) the total missing transverse momentum; (d) the fraction of the τ jet energy carried by the leading track and (e) the number of tracks in the azimuthal hemisphere containing the τ candidate. Symbols correspond to data events and histograms to SM simulation.

6. the fraction of the τ-jet energy carried by the leading track and the energy deposition fraction f_{em} in the LAr electromagnetic section of the τ-jet are such that $f_{em}+E_{track}/E_{\tau-jet} < 1.5$; f_{em} must moreover verify $f_{em} < 0.95$;

7. at most two vertex fitted tracks have to be found in the azimuthal hemisphere containing the τ jet candidate, $N_{tracks,\tau-hem} \leq 2$.

Cuts (1) to (3) ensure a preselection of τ + jet events at high P_T; low Q^2 NC DIS is suppressed by cut (3). At this stage, 372 events are selected in the data while 363.4 are expected from NC DIS and γp processes. Fig. 3a shows, for these selected candidates, the distribution of the polar angle $\theta_{\tau-jet}$ of the τ jet candidate. Photoproduction background, where a low multiplicity jet can fake a τ jet, is seen to contribute mainly at low $\theta_{\tau-jet}$ in contrast with NC DIS background arising when the scattered positron has not been identified. NC DIS contamination at low values of $\theta_{\tau-jet}$ is due to events where the positron has been scattered at large angle through a crack of the calorimeter, and part of the proton remnant has been identified as a high P_T τ jet. Fig. 3b and c show the distributions of the transverse momentum of the τ jet and of the whole final state. Fig. 3d shows the distribution of the maximal fraction of the τ jet energy carried by the vertex fitted tracks found within the identification cone of the τ jet with momentum above 0.15 GeV. The track which maximizes this ratio is defined as the leading track associated with the τ jet candidate. On Fig. 3e the number of tracks $N_{tracks,\tau-hem}$ found in the azimuthal hemisphere containing the τ jet is shown. These two last variables, which are used in the next steps of the selection, are shown to be well described by the simulation.

NC DIS and γp backgrounds are further reduced by requirements (4) to (7). Cut (4) avoids regions close to ϕ cracks of the calorimeter and hence suppresses NC DIS background. Cut (5) efficiently reduces γp background where a low multiplicity jet could fake a τ-jet. Cut (6) ensures a powerful suppression of NC DIS background events where the scattered positron has not been identified. It exploits the fact that the electromagnetic fraction of a τ-jet is high mainly when the τ lepton decays to $n\pi^0 + X$, which generally implies a small value for the ratio E_{track}/E_{jet}. On the contrary, for NC DIS events where the positron has been lost in a crack of the calorimeter, this ratio is expected to peak at one. Fig. 4 illustrates this property of τ jets and shows how cut (6) discriminates the searched signal from the DIS background. The remaining γp contamination is further reduced by the more stringent requirement on track multiplicity imposed by cut (7).

We observe 28 events satisfying the above inclusive τ + jet requirements, which agrees well with the mean expectation of 23.7 ± 5.7 events coming from NC DIS and γp processes.

Additional cuts relevant for the specific search for $LQ \rightarrow \tau +$ jet are then applied :

- a total transverse momentum $P_{T,miss} > 10$ GeV ;
- the τ jet candidate is at $\Delta\phi_{\tau-h} > 165°$ from the total hadronic flow.

Both these cuts exploit the fact that neutrino(s) emerging from the τ decay are collimated with the τ jet direction, and that the other jet in $LQ \rightarrow \tau +$jet events is formed by the fragmentation of a quark and thus should not contribute to the missing transverse momentum. The correlation between the $P_{T,miss}$ and the $\Delta\phi_{\tau-h}$ for the 28 data events which satisfy the criteria (1) to (7) is shown in Fig. 5. We observe no candidate satisfying the additional cuts designed specifically for leptoquark decays involving third generation leptons for an expectation of 0.8 ± 0.3 event from misidentified electrons in NC DIS processes.

It should be noted that the absence of τ + jet events accompanied by a large $P_{T,miss}$ in the hadronic decay modes of the τ makes it rather unlikely for the μ's in the $e^+p \rightarrow \mu^+X$

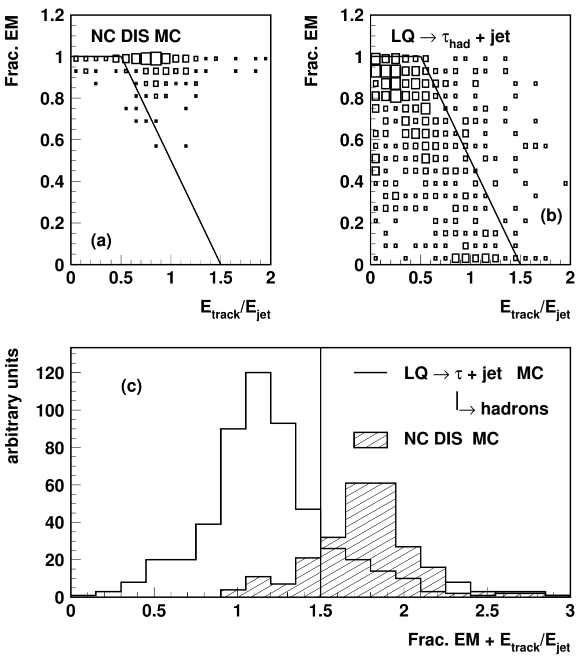

Figure 4: Correlation between the electromagnetic fraction of the τ-jet candidate and the fraction of the jet energy carried by the leading track for (a) NC DIS and (b) $LQ \rightarrow \tau + q$ simulated events; (c) the sum of these variables and the cut applied.

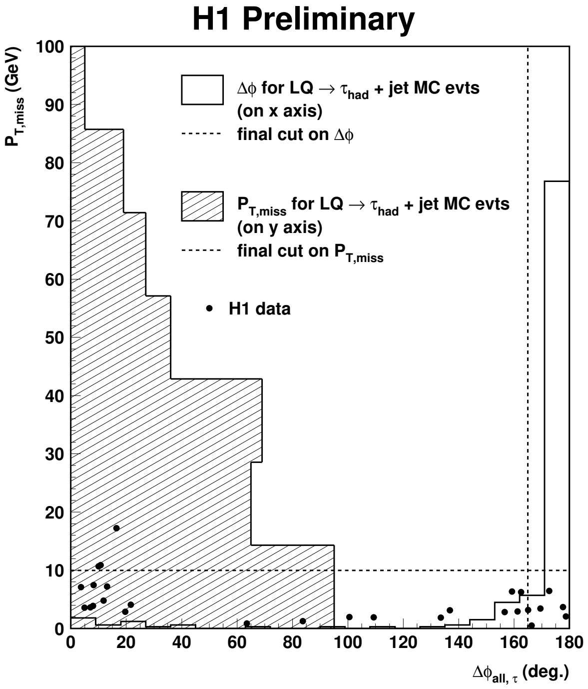

Figure 5: Correlation between the missing transverse momentum $P_{T,miss}$ and the azimuthal angular opening $\Delta\phi_{\tau-h}$ between the τ candidate and the hadronic energy flow; $\bullet$ symbols correspond to data events satisfying cuts (1) to (7); white and hatched histograms show the projections on x and y axis respectively of the expected distributions of $P_{T,miss}$ and $\Delta\phi_{\tau-h}$ for $LQ \rightarrow \tau + jet$ Monte Carlo events.

events [31] to originate from leptonic decays of τ's. Conversely, these muon events fail significantly the kinematic requirements of a two body decay $LQ \rightarrow q + \tau$ followed by a $\tau \rightarrow \mu^+\nu_\mu\bar{\nu}_\tau$ decay since the final state μ^+ would appear boosted in the τ direction and the $\Delta\theta$-$\Delta\phi$ restrictions of Fig. 2 would still apply.

6 Comparison of DIS-like Data with Standard Model Expectation

Fig. 6a and 6b show the projected M_e and y_e distributions of the selected events at "low" Q^2 (2500 GeV^2 $< Q_e^2 <$ 15000 GeV^2) and Fig. 6c and 6d at "high" Q^2 ($Q_e^2 >$ 15000 GeV^2). The distributions of the data are well reproduced by standard DIS predictions in the low Q^2 range. At high Q^2 the data exceed the NC DIS expectation at M_e $\sim$ 200 GeV. Fig. 6e and 6f show the y_e distributions for M_e values below and above 180 GeV. At high M_e and large y_e the experiment tends to exceed the SM expectation.

Fig. 7a shows for the NC selection the measured Q_e^2 distribution in comparison with the expectation from standard NC DIS processes. Also shown in Fig. 7b is the ratio of the Q_e^2 distribution to the NC DIS expectation. The errors resulting from the convolution of the statistical error of the Monte Carlo sample and the systematic errors are correlated for different Q_e^2 bins and are indicated in Fig. 7b. as lines above and below unity joining the $\pm 1\sigma$ errors evaluated at the centre of each bin. These errors are dominated by the uncertainty in the electromagnetic energy scale of the calorimeter and vary between 8.5% at low Q_e^2 and 30% at the highest values of Q_e^2. The NC DIS expectation agrees well with the data for $Q_e^2 \lesssim 10000$ GeV^2 while at larger Q_e^2, deviations are observed, with a slight deficit around Q^2 $\sim$ 15000 GeV^2 and a number of observed events at $Q^2 \gtrsim 15000$ GeV^2 in excess of the NC DIS expectation. Similar plots are

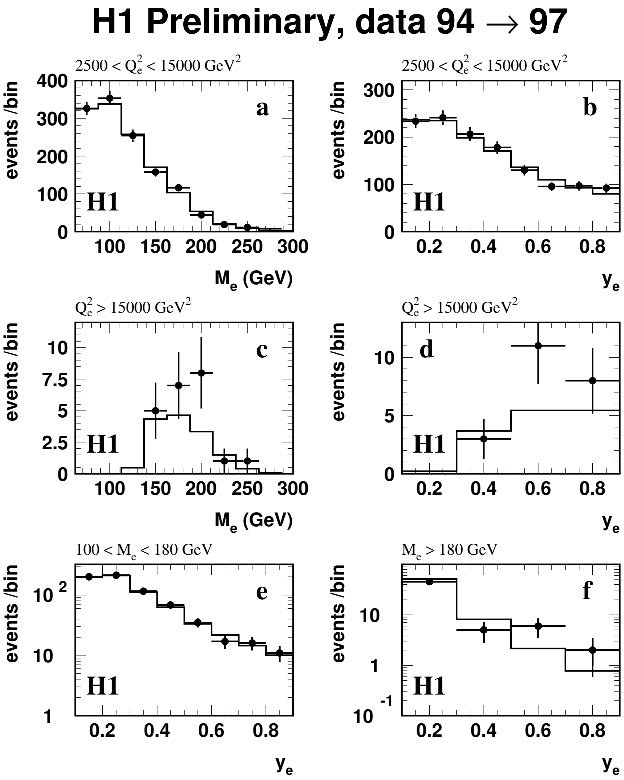

Figure 6: Distributions of M_e and y_e for selected NC DIS candidate events, (a) and (b) for 2500 GeV^2 $< Q_e^2 <$ 15000 GeV^2, (c) and (d) for $Q_e^2 > 15000$ GeV^2; distribution of y_e (e) for $100 < M_e < 180$ GeV and (f) for $M_e > 180$ GeV; superimposed on the data points (• symbols) are histograms of the expectation of standard NC DIS.

shown in Fig. 7c,d for 1997 data alone which suggests similar deviations but now with marginal significance.

To quantify the excess at the highest Q^2, the numbers of observed and expected events with Q_e^2 above various Q^2_{min} values are given in Table 2. It should be noted that the NC DIS expectation per pb $^{-1}$ has increased slightly when compared to [1] due to the wider $\sum(E - P_z)$ range and lower E_T^e cut which improve the acceptance mostly at high y_e. This effectively translates here into a slightly more conservative NC DIS expectation for a given Q^2_{min}. Also given in Table 2 are the Poisson probabilities $\mathcal{P}(N \geq N_{obs})$ that in a random set of experiments the number of NC DIS events N fluctuates to values equal to or larger than the observed number of events N_{obs}.

Fig. 8a shows the measured and expected M_e distributions and Fig. 8b the ratio of the measured M_e distribution to NC DIS expectation for a minimum y_e value of $y_{min} = 0.4$. An excess of events over the NC DIS expectation at the highest mass (~ 200 GeV) still remains. In the mass range 200 GeV $\pm\ \Delta M/2$ with $\Delta M = 25$ GeV, $N_{obs} = 8$ events are observed for an expectation of $N_{DIS} = 3.0 \pm 0.5$. Of the observed events, 5 originate from the $1994 \rightarrow 96$ data (38% of $\mathcal{L}$) and 3 from the 1997 data (62% of $\mathcal{L}$). Hence, no significant excess is seen in the mass spectrum for the 1997 data alone and the "clustering" around $M_e \sim 200$ GeV is, overall, less significant than that observed with $1994 \rightarrow 96$ data only. However, at very large mass ($M_e > 180$ GeV) and for "backscattered" positrons (i.e. $\theta_e^* < 90°$ or equivalently $y_e > 0.5$), we observe in the 1994→96 data $N_{obs} = 4$ in slight excess of the expectation of $N_{DIS} = 1.19 \pm 0.17$

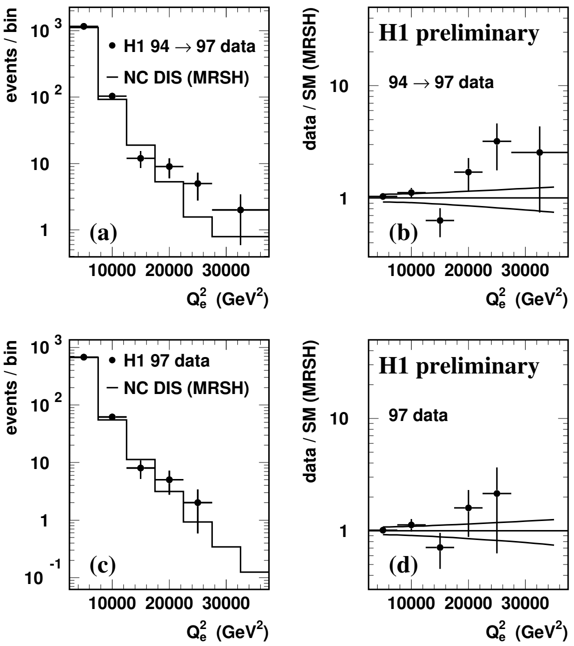

Figure 7: (a) Q_e^2 distribution of the selected NC DIS candidate events for the data (● symbols) and for standard NC DIS expectation (histogram); (b) ratio of the observed and expected number of events as a function of Q_e^2; the lines above and below unity specify the $\pm 1\sigma$ levels determined using the combination of statistical and systematic errors of the NC DIS expectation; (c) and (d) : as (a) and (b) but for 1997 data alone.

while a slight excess is also seen in the 1997 data alone with $N_{obs} = 4$ and $N_{DIS} = 1.75 \pm 0.25$.

It should be emphasized here that N_{obs} and N_{DIS} are conservatively quoted for the same $\Delta M - \Delta y$ region where the most significant excess was observed in the original analysis of the $1994 \rightarrow 96$ data [1] despite the fact that the individual events are slightly (within originally estimated systematic errors) displaced in the $M - y$ plane. It was explicitly checked that repeating exactly the 1994→96 analysis of [1] but using the new *in situ* energy calibration leaves the statistical significance and the physics messages of [1] unchanged. In this domain, 7 events were observed in [1] for an expectation of 0.95 ± 0.18. The estimated mass of one of these 7 events (run # 88999, event # 106218) in which the positron lies within $1^\circ <\mid \phi_e - \phi_{crack} \mid < 2^\circ$ was and remains measured outside this mass region when using the 2α-method in contrast to

Q^2_{min}(GeV^2)	2500	5000	10000	15000	20000	30000
N_{obs}	1297	322	51	22	10	2
N_{DIS}	1276 ± 98	336 ± 29.6	55 ± 6.4	14.8 ± 2.1	4.39 ± 0.73	0.58 ± 0.11
$\mathcal{P}(N > N_{obs})$	42%	56%	60%	5.9%	1.8%	11%

Table 2: Number of observed (N_{obs}) and expected NC DIS (N_{DIS}) events with 4-momentum transfer squared Q_e^2 above given thresholds (Q^2_{min}); $\mathcal{P}(N \geq N_{obs})$ is the probability that the number of NC DIS events fluctuates to values equal to or larger than N_{obs} in a random set of experiments.

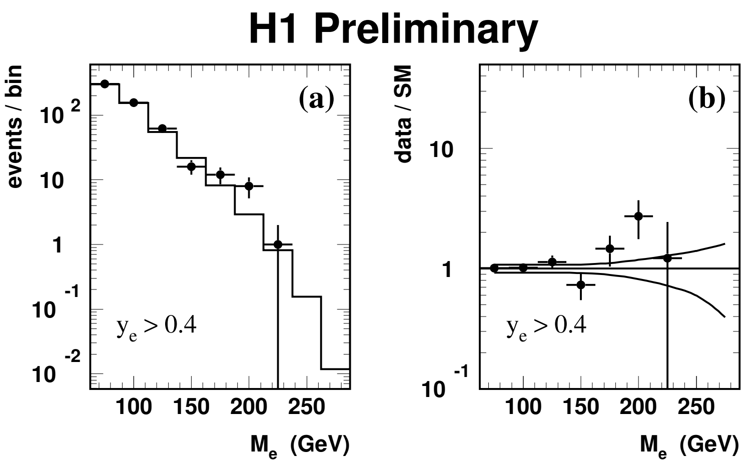

Figure 8: (a) Distribution of M_e for the observed (• symbols) NC DIS candidates with $y_e > 0.4$; the expectation from standard NC DIS is shown as the superimposed histogram; (b) ratio of the observed and expected numbers of events as a function of M_e for $y_e > 0.4$; the lines above and below unity specify the $\pm 1\sigma$ levels of uncertainty for the standard NC DIS expectation using the combination of statistical and systematic errors.

the e-method used in [1] or other kinematic methods discussed in [4]. The 6 other outstanding events of [1] are measured here at M_e values on average 2.4% higher due to the the new *in situ* calibration of the electromagnetic section LAr calorimeter (see section 3) and, thus, one event (run # 122145, event # 69506) has now migrated to $M_e = 216$ GeV.

Fig. 9 shows for the CC selection the measured Q_h^2 distribution in comparison with the standard DIS CC expectation. The systematic errors are relatively large and dominated by the uncertainty on the hadronic energy scale of the calorimeter. Table 3 gives the number of observed and expected CC events, as well as the Poisson probability $\mathcal{P}(N \geq N_{obs})$, for increasing values of Q^2_{min}. In the kinematic region $Q_h^2 > 15000$ GeV^2, there are $N_{obs} = 9$ observed events compared with an expectation of 5.07 ± 2.8 from standard CC DIS.

Q^2_{min}(GeV^2)	2500	7500	15000
N_{obs}	100	41	9
N_{DIS}	95.3 ± 16.7	27.6 ± 8.4	5.07 ± 2.8
$\mathcal{P}(N > N_{obs})$	40%	9%	17%

Table 3: Number of observed (N_{obs}) and expected CC DIS events (N_{DIS}) with 4-momentum transfer squared Q_h^2 above given Q^2_{min} values; $\mathcal{P}(N \geq N_{obs})$ is the probability that the number of CC DIS events fluctuates to values equal to or larger than N_{obs} in a random set of experiments.

7 Constraints on First Generation Leptoquarks

The comparison of the measured mass spectrum with SM predictions is shown in Fig. 10a for the NC DIS analysis. The measured and expected spectra are seen before and after applying a mass dependent y_e cut varies from $\simeq 0.6$ around $M_e = 60$ GeV to $\simeq 0.4$ around $M_e = 200$ GeV, and down to $y_e \simeq 0.2$ at $M_e \gtrsim 250$ GeV.

This cut is designed [7] via Monte Carlo studies to optimize the signal significance for scalar leptoquark searches, given the expected background. It exploits the specific angular dependence of the scalar LQ signal and of the NC DIS background recalled in section 2. After applying the y_e cut, we observe 312 events in the mass range $M_e > 62.5$ GeV while 306 ± 23 are expected. The observed mass spectrum is seen to be well described by the SM expectation. In the mass range 200 GeV $\pm \Delta M/2$ with $\Delta M = 25$ GeV, the same 8 events already discussed in section 6 are observed since the mass dependent y_{cut} optimized for the leptoquark search is $y_{cut} \simeq 0.4$ for $M \simeq 200$ GeV.

For CC DIS-like final states, 210 events are selected in the mass range $M_h > 50$ GeV, which agrees well with the CC DIS expectation of 193.7 ± 28.5. The observed and expected mass spectra are shown to be in good agreement in Fig. 10b. Also shown in Fig. 10c is the ratio of the measured mass distribution to the CC DIS expectation, together with the $\pm 1\sigma$ error band determined using the combination of statistical and systematic errors of the expectation. No significant deviation from the SM expectation is found in the mass spectrum for CC DIS-like channel.

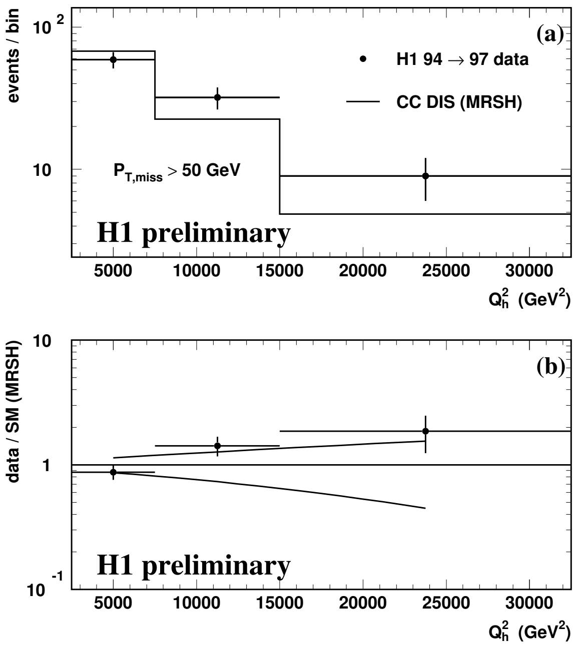

Figure 9: (a) Q_h^2 distribution of the selected CC DIS candidate events for the data (• symbols) and for standard CC DIS expectation (histogram); (b) ratio of the observed and expected number of events as a function of Q_h^2; the lines above and below unity specify the $\pm 1\sigma$ levels determined using the combination of statistical and systematic errors of the CC DIS expectation.

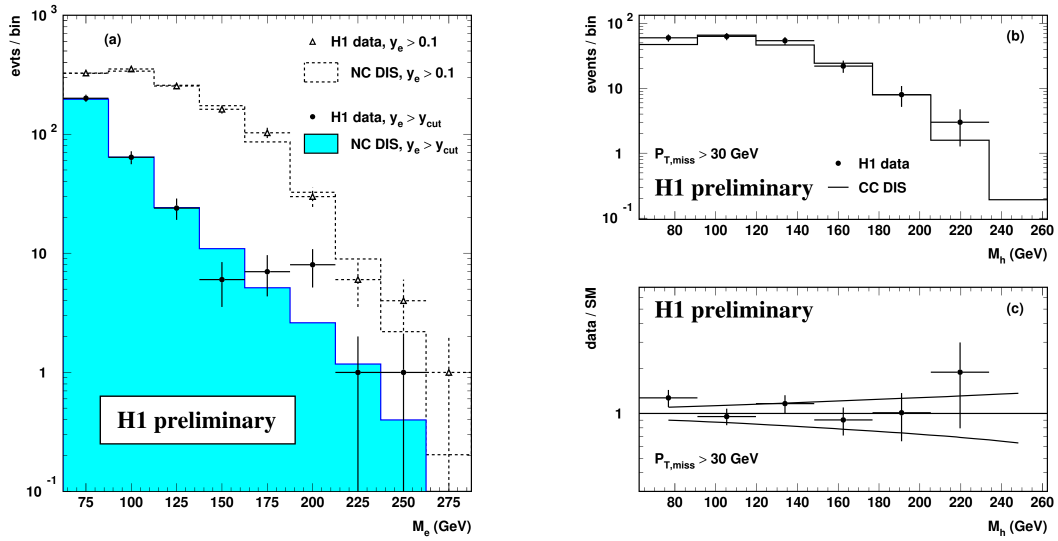

Figure 10: Mass spectra for (a) NC DIS-like and (b) CC DIS-like final states for data (symbols) and DIS expectation (histogram); (c) Ratio of the observed and expected number of events as a function of M_h for CC DIS final states; the lines above and below unity show the $\pm 1\sigma$ error band combining statistical and systematic errors of the CC DIS expectation.

Assuming that the observed excess of events in the NC DIS-like channel is either due to a statistical fluctuation or that the observation contains at most two components (an unknown leptoquark signal and a known expectation from NC DIS) mass dependent constraints can be set on the production cross section of first generation scalar leptoquarks.

The upper limit on the production cross section $\sigma(e^+p \rightarrow LQ)$ as a function of the leptoquark mass is obtained assuming Poisson distributions for the SM background expectation and for the signal. For each contributing channel, we use the branching ratios, the signal detection efficiencies and the numbers of observed and expected events within a mass bin of variable width (adapted to the expected mass resolution) which slides over the accessible mass range. For example, only NC DIS (resp. CC DIS) events with $M_e \in [186; 204]$ GeV (resp. $M_h \in [170; 214]$ GeV) will be used to constrain a 200 GeV leptoquark undergoing a NC (resp. CC) DIS-like decay. The statistical procedure which folds in, channel per channel, the statistical and systematic errors is described in detail in [7]. In addition to the systematic errors on the SM expectations described in section 4, the following uncertainties have been considered to derive exclusion limits on the cross section $\sigma(e^+p \rightarrow LQ)$:

- the lack of knowledge on the proton structure leads to an uncertainty on the signal cross section which is $\simeq 5\%$ for leptoquarks coupling to e^+u, and varies between $\simeq 5\%$ at low masses up to $\simeq 20\%$ around 250 GeV for leptoquarks coupling to e^+d;
- choosing Q_e^2, or $P_{T,e}^2$ instead of M_{LQ}^2 as the hard scale at which the parton distributions are estimated implies an uncertainty of $\pm 7\%$ on the cross section $e^+ + q \rightarrow LQ \rightarrow e^+ + q$, and thus on the leptoquark production cross section;
- the effect of the interference between standard NC DIS and $e^+ + q \rightarrow LQ \rightarrow e^+ + q$ process has been studied and was found negligible.

The signal detection efficiencies are typically determined over a coupling-mass grid with steps in mass of 25 GeV and for coupling values corresponding roughly to the expected ultimate sensitivity to properly take into account the effect on the cross section of the intrinsic width of the searched resonance. Detailed Monte Carlo simulation of about 500 events per point on the grid is performed followed by the application of the full analysis chain. For leptoquarks undergoing NC DIS-like decays, signal detection efficiency is found to vary between 35% at 75 GeV, $\simeq 50\%$ around 200 GeV and 70% at 250 GeV. In the CC DIS-like decay channel, this efficiency ranges between $\simeq 27\%$ for a 75 GeV leptoquark, $\simeq 57\%$ at 100 GeV and reaches 78% at 200 GeV. For leptoquarks in the low mass range undergoing CC DIS-like decays, the limited efficiency is due to the high $P_{T,miss}$ requirement.

Besides the observed and expected numbers of events and signal detection efficiencies, the upper limit on the leptoquark production cross section σ_{LQ} depends only on the branching ratios of the LQ into the channels considered. Hence, assuming a specific LQ model (e.g. [6]) in which $\beta_e = BR(LQ \to eq)$ is known, upper limits on σ_{LQ} can be translated into mass dependent limits on the Yukawa coupling λ_{11}. On the other hand, assuming a given value for the coupling λ_{11}, mass dependent limits on the branching ratio β_e can be derived. These two approaches are addressed in the following.

7.1 Mass dependent limits on the Yukawa coupling

We first consider the BRW model described in section 2. The values of β_e for the different leptoquarks are then known and given in table 1. Rejection limits at 95% confidence level (CL) have been derived from the NC DIS analysis for LQ species predicted by this model and are given in Fig. 11a for leptoquarks having fermionic number $F = 2$ ($e^+ - antiquark$) and in Fig. 11b for those with $F = 0$ which can be produced via a fusion between the e^+ and an incident valence quark. This latter case naturally offers the best sensitivity. For LQ having $F = 0$, these limits represent an improvement by a factor $\simeq 3$ compared to H1 previously published results [7]. For a Yukawa coupling of the electromagnetic strength $\lambda^2/4\pi = \alpha_{EM}$ (i.e. $\lambda \simeq 0.3$), such LQ are excluded at 95% CL up to 275 GeV by this analysis. As can be seen in Fig. 11b the leptoquark $S_{1/2,R}$ is the one for which HERA has the highest sensitivity since both charge states can be produced via a fusion e^+u or e^+d. On the contrary, only an e^+u (resp. e^+d) fusion is possible for the production of $S_{1/2,L}$ (resp. $\tilde{S}_{1/2,L}$), for which the cross sections are thus smaller. For $F = 2$ leptoquarks, the improvement compared to our previous published results is less substantial since e^-p data collected in 1994 had been also taken into account in [7]. These LQ will be best probed with the forthcoming e^-p data taking starting in 1998.

$S_{1,L}$ and $S_{0,L}$ leptoquarks being allowed to undergo CC DIS-like decays with a branching ratio $\beta_\nu = BR(LQ \to \nu q) = 0.5$, the combination of NC and CC DIS analysis is expected to better constrain these leptoquarks. The result of this combination is given for the $S_{0,L}$ by the curve $\beta_e = \beta_\nu = 0.5$ in Fig. 12 (dash-dotted line). It can be seen that combining the two contributing channels improves the sensitivity on $S_{0,L}$ up to that achieved on $S_{0,R}$, recalled on Fig. 12 by the curve $\beta_e = 1$ (dotted line).

The DELPHI [32] and OPAL [33] experiments at LEP recently performed a search for single leptoquarks using data accumulated at centre of mass energies of 161 and 172 GeV. For a Yukawa coupling of the electromagnetic strength, the best resulting limit of 142 GeV [32] is not yet competitive with the sensitivity achieved at HERA. Comparisons of our results with limits

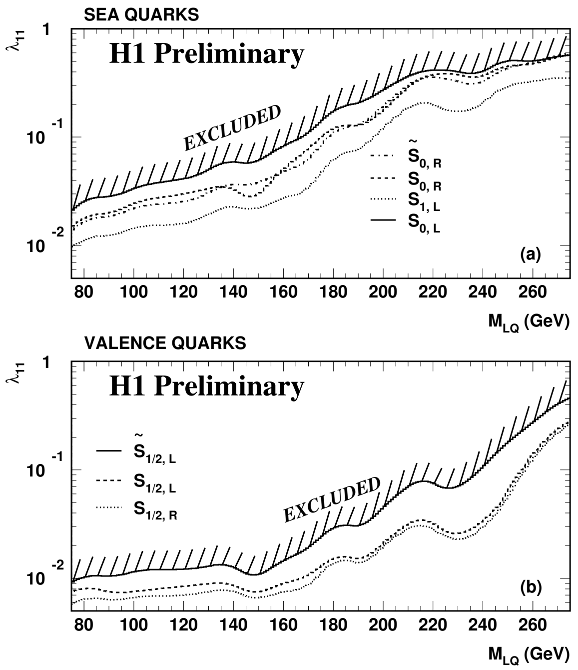

Figure 11: Exclusion limits at 95% CL on the Yukawa coupling λ as a function of the leptoquark mass (a) for $F = 2$ and (b) $F = 0$ scalar leptoquarks described by BRW model. Domains above the curves are excluded.

obtained at the TeVatron collider will be presented in section 7.2.

Moving away from the BRW model, we now consider scalar leptoquarks that can undergo both NC and CC DIS-like decays, β_e and β_ν being free parameters. By gauge invariance this only concerns LQ coupling to $e^+\bar{u}$. As an example, the 95% CL exclusion contour for a LQ decaying with $\beta_\nu = 90\%$ in νq and $\beta_e = 10\%$ in eq is shown in Fig. 12 as the full line. The gain obtained by the combination of both channels can be seen when comparing this contour with the greyed domain showing the sensitivity achieved using only NC DIS-like channel. For $\beta_\nu = 90\%$ and $\beta_e = 10\%$, LQ masses below 210 GeV are excluded at 95% CL by our analysis, for Yukawa couplings of the electromagnetic strength. This extends far beyond the domain excluded by TeVatron experiments [34, 35] which for such small values of β_e only exclude scalar leptoquark masses below $\simeq 110$ GeV. With an e^- incident beam, HERA sensitivity on such leptoquarks, which then can be produced via a fusion with a *valence* u-quark, will be considerably enhanced. Hence a large discovery potential is opened for HERA, for high mass leptoquarks decaying in νq with a high branching ratio.

7.2 Mass dependent limits on $\beta(LQ \to eq)$

We consider here leptoquarks which undergo NC DIS-like decays with a branching ratio β_e and do not make any assumption on the other possible decay modes of the LQ. For a fixed value of the Yukawa coupling λ_{11} upper limits on LQ production cross section are translated in terms of mass dependent limits on the branching β_e. Results are shown in Fig. 13a,b for LQ produced

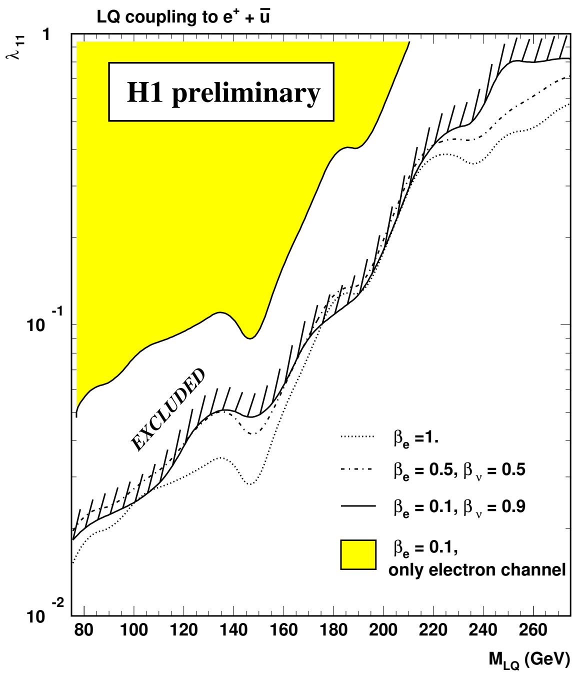

Figure 12: Exclusion limits at 95% CL on the Yukawa coupling λ as a function of the leptoquark mass for scalar leptoquarks produced via $e^+\bar{u}$ fusion. Different hypothesis for the branching ratios into eq, νq are considered. Domains above the curves are excluded.

via a e^+d or e^+u fusion respectively. Greyed domains are excluded at 95% CL by our NC DIS analysis. On Fig. 13a, the central limit contour for $\lambda_{11} = 0.1$ has been obtained assuming a constant uncertainty of $\pm 5\%$ on the d quark density distribution. Curves above and below this contour define the error band obtained when d quark density is enhanced/lowered by a factor varying linearly between 5% at low masses and up to 20% at 250 GeV. For LQ coupling to e^+u (Fig. 13b), a constant scaling factor of $\pm 5\%$ has been applied on the quite well-known u density, resulting in a much narrower error band.

For the already small λ_{11} values considered, domains excluded by our analysis extend beyond the region covered by the $D\emptyset$ experiment [34] at TeVatron represented by the hatched domain in Fig. 13, even in the less favourable case of LQ coupling to e^+d. For $\beta_e = 1$ (0.5), scalar LQ masses below 225 GeV (204 GeV) are excluded by $D\emptyset$ independently of the value of the Yukawa coupling[5]. Scalar LQ in the BRW model are thus already severely constrained. However for small values of β_e the current sensitivity of the TeVatron does not reach the high mass domain. For example, as was stated before, masses up to only $\simeq 110$ GeV are excluded by the D∅ experiment if $\beta_e = 10\%$ while this analysis rules out masses below $\simeq 210$ GeV if $\lambda_{11} = 0.1$ independently of other possible decay modes of the leptoquark, as can be seen in Fig. 13b. This limit extends up to 255 GeV for an electromagnetic strength of the Yukawa coupling λ_{11} as shown by the greyed domain in Fig. 14a. Hence the high mass region constitutes an open window for a discovery at HERA, provided that β_e is not too high.

[5]A combination of $D\emptyset$ [34] and CDF [35] results excludes scalar leptoquark masses up to 242 GeV for $\beta_e = 1$ [36].

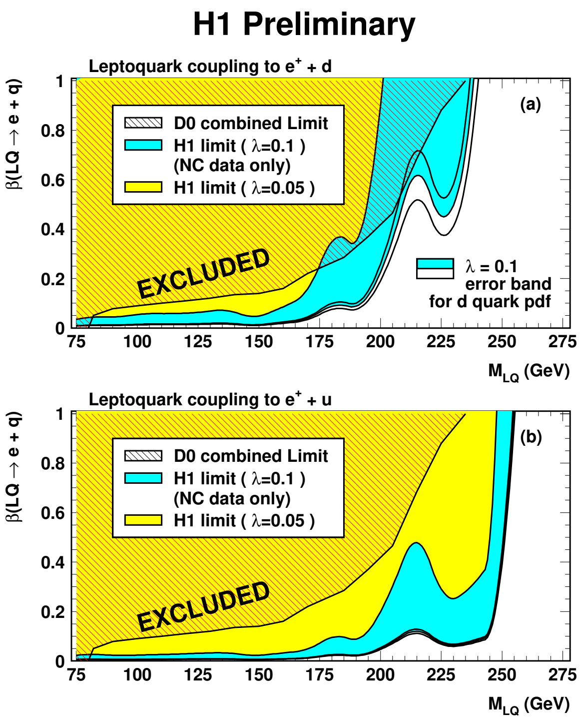

Figure 13: Mass dependent exclusion limits at 95% CL on the branching ratio $\beta_e = BR(LQ \rightarrow eq)$ for scalar leptoquarks produced by (a) e^+d and (b) e^+u fusion. Two exclusion regions corresponding to $\lambda = 0.1$ and $\lambda = 0.05$ are represented as greyed areas. The $D\emptyset$ limit is also shown as hatched region.

8 Constraints on Leptoquarks Coupling to Mixed Generations

We now consider leptoquarks possessing a coupling λ_{11} to first generation lepton-quark pairs as well as a coupling λ_{3j} with leptons of the third generation[6].

The selection cuts described in section 5.2 ensure a detection efficiency on the $LQ \rightarrow \tau + q$ signal which is $\simeq 10\%$ for leptoquark masses of 100 GeV and reaches a plateau at $\simeq 25\%$ above 200 GeV. Mass dependent exclusion limits at 95% CL are shown in Fig. 14a on λ_{11} when fixing the relative branching fractions β_e and β_τ into $e+jet$ and $\tau+jet$ final states, for a generic scalar leptoquark coupling to $e^+ + u$ pairs (such as the $S^*_{1/2,L}$ in the BRW model) and for three different sets of (β_e, β_τ). Here both channels $LQ \rightarrow e^+ + jet$ and $LQ \rightarrow \tau^+ + jet$ are combined. This latter channel is background free but the former benefits from a higher selection efficiency, such that finally both provide a similar sensitivity to the signal. Hence, the limits obtained as soon as $\beta_e + \beta_\tau \simeq 1$ are very similar to that achieved for $\beta_e = 1$. Assuming $\beta_e = 10\%$ and $\beta_\tau = 90\%$, masses below 275 GeV are excluded at 95% CL for an electromagnetic strength of the λ_{11} coupling, as shown in Fig. 14a. Such situations with small β_e and high β_τ are especially interesting for HERA since then the mass domain excluded by the TeVatron does not extend very far. The CDF experiment has performed a search for third generation LQ looking at $\tau\tau bb$ final states [37], and excluded scalar LQ with masses below 99 GeV if $\beta(LQ \rightarrow \tau b) = 1$. A complementary search has been carried out by $D\emptyset$ [38], where the analysis of $\nu\nu bb$ final

[6]Leptoquarks coupling to both eq and $\mu q'$ pairs being very severely constrained [9] by $\mu \rightarrow e\gamma$ and $K \rightarrow e\mu$ processes are not considered in the following.

states leads to a lower mass limit of 94 GeV for $\beta(LQ \to \nu b) = 1$. These constraints are less stringent than the $\simeq 110$ GeV mass limit obtained from TeVatron searches for first generation leptoquarks assuming $\beta_e = 10\%$. Thus an important discovery potential is open at HERA for high mass scalar leptoquarks decaying with a small branching ratio in eq and a high branching ratio in τq.

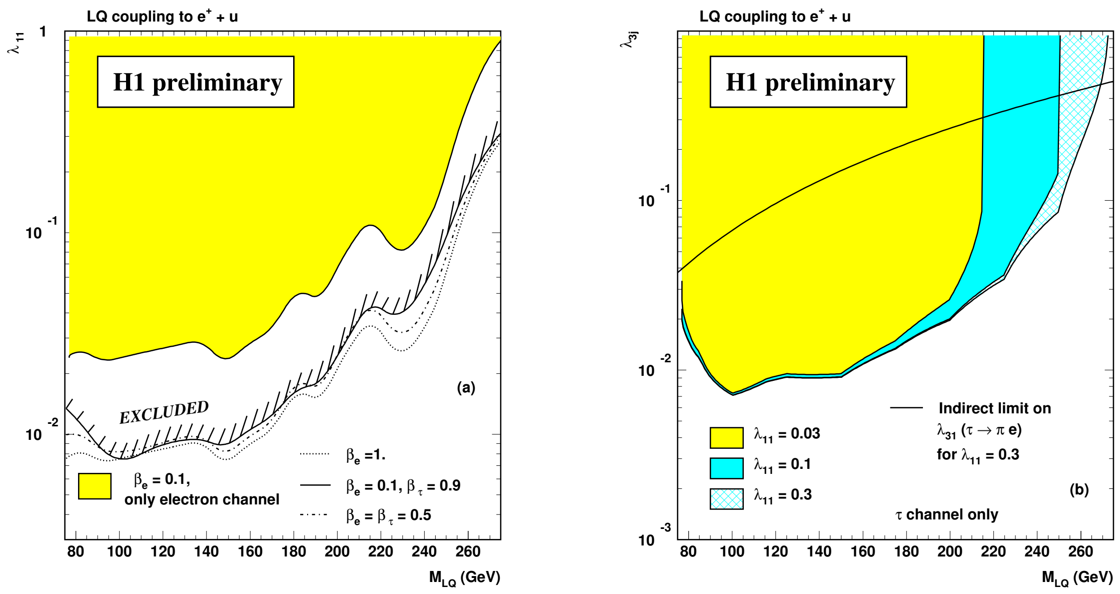

Figure 14: (a) Mass dependent exclusion limits at 95% CL on the Yukawa coupling λ_{11}, for scalar leptoquarks produced by e^+u fusion. Different hypothesis for the branching ratios into eq, τq are considered. Domains above the curves are excluded. (b) Exclusion domains in the plane λ_{3j} $(j = 1, 2)$ against the leptoquark mass for several fixed value of λ_{11} (greyed areas). Mass dependent indirect limit on λ_{31} is also represented as the dotted line.

An alternative representation of our results is given in Fig. 14b in the plane λ_{3j} against the leptoquark mass, for different fixed values of λ_{11}. We consider here a leptoquark formed via e^+u fusion such that only couplings λ_{3j} with $j = 1, 2$ are relevant and make the additional assumption that $\beta_e + \beta_\tau = 1$. Greyed domains are excluded at 95% CL by the τ + jet final states analysis. For $\lambda_{11} = 0.3$, masses below 215 GeV are already excluded by the analysis in the $e + q$ channel while, for the smaller λ_{11} considered in Fig. 14b, the $\tau + jet$ analysis allows to explore an uncovered domain for masses above $\simeq 80$ GeV. For both couplings λ_{11} and λ_{3j} of the electromagnetic strength, such leptoquarks lighter than 255 GeV are excluded at 95% CL. This limit goes down do 237 GeV for leptoquarks formed by e^+d fusion. A similar lepton flavour violation analysis has been carried out by ZEUS Collaboration in [39] with an integrated luminosity of $\simeq 3$ pb $^{-1}$. For $\lambda_{11} = \lambda_{3j} = 0.03$, the analysis presented here extends the mass range excluded in [39] by $\simeq 65$ GeV. Also shown in Fig. 14b is the best indirect limit [9] on λ_{31} in the case $\lambda_{11} = 0.3$. This indirect constraint comes from the upper limit on the branching ratio $BR(\tau \to \pi^0 e)$ which could be affected by the process $\tau \to d + LQ$ followed by the $e + d$ decay of the virtual leptoquark. The H1 direct limit improves this indirect constraint by typically one order of magnitude. No low energy process constrains the coupling λ_{32} in this case. Thus there is an unexplored domain which is covered by H1 in the plane λ_{32} against the leptoquark mass.

It should be noted however that other leptoquark species can be constrained more severely by measurements of indirect processes. This is in particular the case for a leptoquark coupling to

e^+d pairs (as $\tilde{S}_{1/2,L}$ in BRW model), for which the three couplings λ_{31}, λ_{32}, λ_{33} are constrained respectively by $\tau \rightarrow \pi^0 e$, $\tau \rightarrow K^0 e$ and $B \rightarrow \tau e X$ [9]. Such a leptoquark presents the same characteristics as a $\tilde{u}_L^j$ squark in supersymmetric models where R-parity is violated by couplings λ'_{1j1} (analogous to λ_{11}) and λ'_{3jk} (analogous to λ_{3k}). Exclusion domains which have been derived in [40] in the plane λ'_{3jk} against the squark mass make it again possible to conclude that H1 direct limits extend far beyond the sensitivity achieved by low energy phenomena.

9 Conclusions

We have compared the dependences in Q^2, in the electron-parton centre of mass energy $M = \sqrt{xs}$ and in the final state lepton angular distribution y in high Q^2 neutral (NC) and charged current (CC) data to Standard Model expectations for deep inelastic scattering (DIS). We found that the deviations in the Q^2 spectrum previously observed in the 1994→1996 data at $Q^2 \gtrsim 15000$ GeV^2 remain, with a slight deficit around $Q^2 \sim 15000$ GeV^2 and an excess over the NC DIS expectation at $Q^2 \gtrsim 15000$ GeV^2. The discrepancies observed in the 1997 data alone are nevertheless of marginal significance. No significant clustering in the mass spectra is observed with the 1997 data alone.

A search for new bosons possessing couplings to lepton-quark pairs was performed assuming either a unique Yukawa coupling involving first generation leptons or the existence of mixed couplings involving the μ or the τ lepton. For first generation leptoquarks, masses up to 275 GeV are ruled out by the present analysis for an electromagnetic strength of the Yukawa coupling if the branching ratio $\beta_e = BR(LQ \rightarrow eq) = 1$. This limit still extends to 255 GeV for β_e as small as 10%, which extends far beyond the domain presently covered at other colliders. No candidate for $LQ \rightarrow \mu + jet$ and $LQ \rightarrow \tau + jet$ has been observed and constraints have been set on the Yukawa coupling involving the τ lepton for a mass range extending far beyond the previously existing limits.

Acknowledgements

We are grateful to the HERA machine group whose outstanding efforts made this experiment possible. We appreciate the immense effort of the engineers and technicians who constructed and maintain the detector. We thank the funding agencies for their financial support of the experiment. We wish to thank the DESY directorate for the hospitality extended to the non-DESY members of the collaboration.

References

[1] H1 Collaboration, C. Adloff *et al.*, Z. Phys. C74 (1997) 191.

[2] ZEUS Collaboration, J. Breitweg *et al.*, Z. Phys. C74 (1997) 207.

[3] M. Drees, Phys. Lett. B403 (1997) 353.

[4] U. Bassler and G. Bernardi, Z. Phys. C76 (1997) 223.

[5] T.K. Kuo and T. Lee, Mod. Phys. Lett. A12 (1997) 2367; K.S. Babu *et al.*, Phys. Lett. B402 (1997) 367; J.L. Hewett and T.G. Rizzo, Phys. Lett. B403 (1997) 353; Z. Kunszt and W.J. Stirling, Z. Phys. C75 (1997) 453; T. Plehn *et al.*, Z. Phys. C74 (1997) 611; C. Friberg, E. Norrbin and T. Sjöstrand, Phys. Lett. B403 (1997) 329; J.K. Elwood and A.E. Faraggi, Nucl. Phys. B512 (1998) 42; M. Heyssler and W.J. Stirling, Phys. Lett. B407 (1997) 259; J. Blümlein, Proceed. of the 5th Int. Workshop on Deep Inelastic Scattering and QCD (DIS 97), Chicago, USA (14-18 April 1997) 5pp.; E. Keith and E. Ma, Phys. Rev. Lett. 79-22 (1997) 4318; N.G. Deshpande and B. Dutta, Phys. Lett. B424 (1998) 313; J.L. Hewett and T.G. Rizzo, SLAC preprint PUB-7549 (August 1997) 45pp.; T.G. Rizzo, Proceed. of the Workshop on Physics Beyond the Desert 1997, Tegernsee, Germany (8-14 June 1997) 32pp.; Z. Xiao, RAL preprint TR-97-043 (September 1997) 26pp.; R. Ruckl and H. Spiesberger, Proceed. of the Workshop on Physics Beyond the Desert, Tegernsee, Germany (8-14 Jun 1997) 18pp.; M. Sekiguchi, H. Wada and S. Ishida, Nihon Univ. preprint NUP-A-97-23 (December 1997) 7 pp.

[6] W. Buchmüller, R. Rückl and D. Wyler, Phys. Lett. B191 (1987) 442.

[7] H1 Collaboration, I. Abt *et al.*, Nucl. Phys. B396 (1993) 3; *ibid*, T. Ahmed *et al.*, Z. Phys. C64 (1994) 545; *ibid*, T. Ahmed *et al.*, Phys. Lett. B369 (1996) 173.

[8] ZEUS Collaboration, M. Derrick *et al.*, Phys. Lett. B306 (1993) 173.

[9] S. Davidson, D. Bailey and B. Campbell, Z. Phys. C61 (1994) 613.

[10] M. Leurer, Phys. Rev. D49 (1994) 333; *ibid.* D50 (1994) 536.

[11] B. Schrempp, Proc. of the Workshop Physics at HERA, DESY, Hamburg (1991), vol. 2 p. 1034, and references therein.

[12] H1 Collaboration, I. Abt *et al.*, DESY preprint 93-103 (July 1993) 194pp.; *idem* DESY Internal Report H1-96-01 (March 1996) 157pp.; *idem* Nucl. Instr. and Meth. A386 (1997) 310.

[13] H1 Calorimeter Group, B. Andrieu *et al.*, Nucl. Instr. and. Meth. A336 (1993) 460.

[14] H1 Calorimeter Group, B. Andrieu *et al.*, Nucl. Inst. and Meth. A344 (1994) 492.

[15] H1 Calorimeter Group, B. Andrieu *et al.*, Nucl. Instr. and. Meth. A350 (1994) 57; *idem*, Nucl. Instr. and. Meth. A336 (1993) 499.

[16] H1 SPACAL Group, R.D. Appuhn *et al.*, Nucl. Instr. and Meth. A386 (1997) 397.

[17] H1 BEMC Group, J. Ban *et al.*, Nucl. Instr. and Meth. A372 (1996) 399.

[18] Ph. Bruel, Ph.D Thesis, Université de Paris-Sud, "Recherche d'intéractions au-dela du Modele Standard" (in French)

[19] A.D. Martin. W.J. Stirling and R.G. Roberts, Phys. Lett B306 (1993) 145; *ibid.* B309 (1993) 492.

[20] V.N. Gribov et L.N. Lipatov, Sov. Journ. Nucl. Phys. 15 (1972) 78;
G. Altarelli et G. Parisi, Nucl. Phys. B126 (1977) 298;
Y.L. Dokshitzer, JETP 46 (1977) 641.

[21] DJANGO 6.2; G.A. Schuler and H. Spiesberger, Proc. of the Workshop Physics at HERA, W. Buchmüller and G. Ingelman (Editors), (October 1991, DESY-Hamburg) Vol. 3 p. 1419.

[22] HERACLES 4.4; A. Kwiatkowski, H. Spiesberger and H.-J. Möhring, Comput. Phys. Commun. 69 (1992) 155.

[23] ARIADNE 4.08; L. Lönnblad, Comput. Phys. Commun. 71 (1992) 15.

[24] G. Gustafson and U. Pettersson, Nucl. Phys. B306 (1988) 746; *idem*, *addendum* Lund University preprint LU-TP-87-19, (October 1987) 4pp.; B. Andersson *et al.*, Z. Phys. C43 (1989) 625.

[25] JETSET 7.3 and 7.4; T. Sjöstrand, Lund Univ. preprint LU-TP-95-20 (August 1995) 321pp; *idem*, CERN preprint TH-7112-93 (February 1994) 305pp.

[26] PYTHIA 5.6; T. Sjöstrand, Comp. Phys. Comm. 39 (1986) 347;
T. Sjöstrand and M. Bengtsson, Comp. Phys. Comm. 43 (1987) 367;
JETSET 7.3; T. Sjöstrand, CERN preprint TH-6488-92 (1992).

[27] M. Glück, E. Reya and A. Vogt, Phys. Rev. D45 (1992) 3986; *idem*, Phys. Rev. D46 (1992) 1973.

[28] LEGO 0.02 and SUSSEX 1.5; K. Rosenbauer, dissertation Aachen (in German), PITHA 95/16, July 1995.

[29] S. Bentvelsen, J. Engelen and P. Kooijman, Proc. of the Workshop Physics at HERA, W. Buchmüller and G. Ingelman (Editors), (October 1991, DESY-Hamburg) Vol. 1 p. 25; K.C. Hoeger, *ibid.* p. 43; and references therein.

[30] A. Blondel, F. Jacquet, Proceedings of the Study of an ep Facility for Europe, ed. U. Amaldi, DESY report 79-48 (1979) 391.

[31] H1 Collaboration, C. Adloff *et al.*, DESY preprint 98-063 (May 1998) (hep-ex/9806009)

[32] DELPHI Collaboration, F. Barao *et al.*, "Searches for Single Leptoquark Production at $\sqrt{s} = 161$ GeV and $\sqrt{s} = 172$ GeV with the DELPHI Detector", Contributed paper to the International Europhysics Conference on High Energy Physics, Jerusalem, Israël (19-26 August 1997), Abstract 352, Pa 11,13,7 Pl 15,17

[33] OPAL Collaboration, "Search for Single Leptoquark Production in Electron-Photon Scattering at $\sqrt{(s)} = 161$ and 172 GeV, Contributed paper # 205 to the Int. Europhysics Conf. on High Energy Physics, Jerusalem, Israël (19-26 August 1997).

[34] D∅ Collaboration, B. Abbott *et al.*, Phys. Rev. Lett. 79 (1997) 4321;
D∅ Collaboration, B. Abbott *et al.*, Phys. Rev. Lett. 80 (1998) 2051.

[35] CDF Collaboration, F. Abe *et al.*, Phys. Rev. Lett. 79 (1997) 4327.

[36] see http://www-d0.fnal.gov/public/new/analyses/lq/lq_mar98.html

[37] CDF Collaboration, F. Abe *et al.*, Phys. Rev. Lett. 78 (1997) 2906.

[38] D∅ Collaboration, B. Abbott *et al.*, FERMILAB-PUB-98-081-E (hep-ex/9803009).

[39] ZEUS Collaboration, M. Derrick *et al.*, Z. Phys. C73 (1997) 613.

[40] H1 Collaboration, "A Search for Squarks of R-Parity Violating SUSY at HERA", Contributed paper # 580 to the XXIX Int. Conf. on High Energy Physics, Vancouver, Canada (23-29 July 1998).